THE JOURNAL OF PHYSICAL CHEMISTRY Letters

Letter

pubs.acs.org/JPCL

Spectroscopic Signature of Stacking Disorder in Ice I

Thomas H. G. Carr,[†] Jacob J. Shephard,[†,‡] and Christoph G. Salzmann*[,†]

[†]Department of Chemistry, University College London, 20 Gordon Street, London WC1H 0AJ, United Kingdom

[‡]Department of Chemistry, Durham University, South Road, Durham DH1 3LE, United Kingdom

ABSTRACT: There is a growing realization that the presence of stacking disorder in ice I strongly influences its physical and chemical properties. Using Raman spectroscopy, we gain new fundamental insights into the spectroscopic properties of ice. We show that stacking disorder can be detected and quantified by comparing the spectra of stacking disordered ice with spectra of the "ordinary" hexagonal ice I*h*. The spectral signature of stacking disorder is thought to arise from a greater structural diversity on the local length scale, vibrational modes that appear due to the lower-symmetry environments, and a strengthening of the covalent bonds. Our findings are compared to results from diffraction and calorimetry, and we discuss the advantages and disadvantages of the three techniques with respect to detecting stacking disorder in ice I. Apart from characterizing stacking disordered ice in the research lab, our new method is perfectly suited for remote or telescopic applications aiming at the identification of stacking disordered ice in nature.

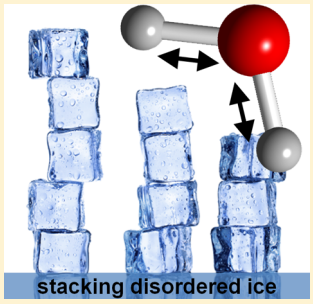

SECTION: Spectroscopy, Photochemistry, and Excited States

Ice is a material of fundamental importance to a vast range of critical processes in geology,[1] biology,[2] chemistry,[3] the atmospheric sciences,[4] and space research.[5] The "ordinary" ice, the phase of ice which crystallizes upon freezing liquid water at 0 °C and atmospheric pressure, is commonly called hexagonal ice or ice I*h*. Using electron diffraction, it was shown in 1943 that a metastable cubic form of ice exists called ice I*c*.[6] In both, ice I*h* and ice I*c*, the water molecules form puckered layers consisting entirely of six-membered rings in the armchair conformation. The structural difference between the two phases lies in the conformations of the six-membered rings that *connect* these layers and therefore affect the way in which the layers are stacked. In the case of ice I*h*, they are in the boat conformation, whereas they are armchair in ice I*c*. Kuhs et al. realized that ice I*c* does not only contain cubic stacking sequences but hexagonal ones as well.[7−9] For this reason, Malkin et al. recently proposed that this material should actually be called stacking disordered ice (ice I*sd*).[10] This name reflects the fact that essentially a continuum of structures with varying fractions of hexagonal/cubic stacking is possible between pure ice I*h* and the so far elusive perfect cubic end member for which the name ice I*c* would be appropriate. A possible stacking sequence in ice I*sd* is shown in Figure 1a. The running oxygen−oxygen coordination number shown in Figure 1b illustrates the subtle structural differences and local density fluctuations that exist in the ice I family beyond the first coordination shell.

The presence of stacking disorder has profound consequences for the physical and chemical properties of ice I (e.g., vapor pressure, crystal growth and shape, light scattering properties, surface chemistry, etc.).[4,10−15] The efficient detection and quantification of stacking disorder has therefore become a high priority, and new techniques are sought that are suited not only for the research lab but also for remote locations, such as the Earth's atmosphere, space, or icy moons and planets. At present, neutron and X-ray diffraction are the most frequently used techniques for quantifying the extent of stacking disorder

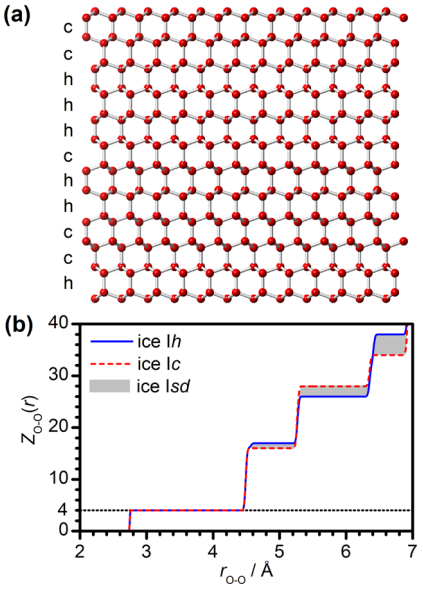

Figure 1. (a) Possible stacking sequence of layers in ice I*sd*. Hexagonal or cubic stacking is indicated by "h" or "c", respectively. Hydrogen atoms have been omitted for clarity. (b) Running oxygen−oxygen coordination number of the pure ice I*h* and I*c* structures. Gray-shaded areas indicate the range of possible values for ice I*sd*. The running coordination number is the average number of oxygen atoms contained within a sphere with oxygen at its center and radius r_{O-O}.

Received: May 19, 2014
Accepted: June 30, 2014
Published: June 30, 2014

in ice in laboratory studies.[7−10,14] Furthermore, the ice I*sd* to ice I*h* phase transition has been shown to cause an exothermic feature in calorimetry.[16−21] The currently prevailing opinion, which we challenge here, is that there are no detectable spectroscopic differences between ice I*h* and ice I*sd*.[22,23]

For this study, several different ice I*sd* samples were prepared by transforming various high-pressure phases of ice at ambient pressure.[7,17,20,24−26] We compare their Raman spectra with those of ice I*h*, and the resulting spectroscopic quantities are contrasted with results from previously reported diffraction and calorimetric studies. The advantages and disadvantages of the individual experimental techniques are discussed on a fundamental level but also with a view toward detecting and characterizing ice I*sd* in nature.

H_2O and D_2O high-pressure phases of ice were prepared by compressing and heating ice I*h* samples in a piston−cylinder setup to the required p/T points in the phase diagram. The samples were subsequently quenched with liquid nitrogen under pressure and recovered at ambient pressure.[27] This included ices II, IX, V, and VIII as well as high-density amorphous ice (HDA).[28] The phase identities of the samples were confirmed by comparing their Raman spectra with spectra in the literature.[29−32] The ice I*sd* samples were then obtained by heating the high-pressure phases from 80 K in vacuo[7,17,20,24−26] followed by immediate cooling back to 80 K once complete conversion had taken place. In the cases of ice VIII and HDA, the phase transitions to ice I*sd* proceed via an intermediate stage of low-density amorphous ice.[28,33]

Figure 2a shows the normalized Raman spectra of H_2O ice I*sd* samples from different parent materials (spectra 2−6) and of H_2O ice I*h* (spectrum 1) in the coupled ν(O−H) spectral region. Obvious spectral differences can be seen upon comparing the spectra of the ice I*sd* samples with the ice I*h* spectrum. These include higher intensities on the low- and high-wavenumber side of the main feature as well as a shift to higher wavenumbers and an overall broadening of the main feature. In the sequence ice I*sd* from HDA (spectrum 2) to ice I*sd* from ice V (spectrum 6), the spectral differences with ice I*h* (spectrum 1) become increasingly more pronounced and are seen most clearly in the difference spectrum.

Very similar spectroscopic trends can be seen in the coupled ν(O−D) spectral region of D_2O ice I*sd* samples and D_2O ice I*h*, as shown in Figure 2b. Again, the intensity on the low- and high-wavenumber side of the main feature is higher for the ice I*sd* samples (spectra 2−4) than for ice I*h* (spectrum 1), and the main feature broadens and shifts to higher wavenumbers. These differences can be seen again most clearly in the difference spectrum.

In the next step, we calculated the integrated areas of the entire spectral features, $A_{\nu(O-H)}$ and $A_{\nu(O-D)}$, which are listed in Figure 2. The integrated areas capture both the increases in the intensities of the shoulders as well as the peak broadening in the ice I*sd* spectra relative to ice I*h*. We propose that these values reflect the amount of stacking disorder present in the ice samples. Figure 3a shows the correlation between the $A_{\nu(O-D)}$ and $A_{\nu(O-H)}$ values of the various samples, which indicates that the amount of stacking disorder in ice I*sd* depends primarily on the identity of the parent material.

To demonstrate that our spectroscopy approach is capable of following the ice I*sd* to ice I*h* phase transition, the H_2O ice I*sd* sample prepared from ice V was heated to increasingly higher annealing temperatures and then recooled to 80 K for spectral analysis. Pronounced changes in $A_{\nu(O-H)}$ occur upon thermal

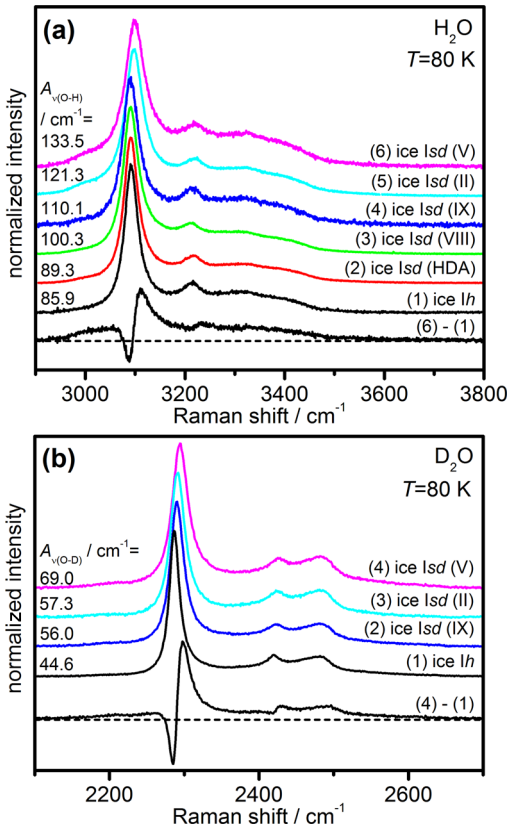

Figure 2. Raman spectra of the coupled (a) ν(O−H) and (b) ν(O−D) stretching regions of H_2O and D_2O ice I*h* and ice I*sd* samples, respectively. The spectra were normalized to the maximum intensity of the most intense feature and shifted vertically for clarity. The parent materials of ice I*sd* are given in parentheses. The bottom spectra in both panels are difference spectra, as indicated. The listed integrated peak areas, $A_{\nu(O-H)}$ and $A_{\nu(O-D)}$, are average values of the spectra shown and typically four additional spectra.

annealing, as shown in Figure 3b, and $A_{\nu(O-H)}$ reaches the value expected for ice I*h* after annealing at 210 K. These spectral changes are in good agreement with calorimetric studies that showed that ice I*sd* from ice V transforms to ice I*h* in this temperature range.[17,20] Furthermore, consistent with results from neutron diffraction,[9] our data indicate that the ice I*sd* to ice I*h* phase transition does not take place at a precisely defined temperature but that it is more a gradual process that depends upon the annealing conditions (i.e., time and temperature).

Using neutron diffraction, the fractions of cubic stacking sequences or "cubicities" of D_2O ice I*sd* samples from ice IX and ice V have been obtained.[8,9,14] (The fraction of hexagonal stacking sequences is 1 − cubicity.) Figure 3c shows that a higher value of $A_{\nu(O-D)}$ is associated with a higher cubicity. It has been suggested that there is a relationship between the features of stacking disorder in diffraction and the exothermicity of the enthalpy values of the ice I*sd* to ice I*h* phase transition.[21] Figure 3d shows that there is also a correlation between our $A_{\nu(O-H)}$ values and the transition enthalpies. The trends shown in Figure 3c and d therefore also suggest that our spectroscopic approach is capable of detecting the extent of stacking disorder in ice I. We note that we have also recently shown that subtle structural relaxation processes in low-density amorphous ice can be followed using Raman spectroscopy.[35]

It is generally accepted that the main feature of the coupled stretching modes in the Raman spectra of ice is caused by the

dx.doi.org/10.1021/jz500996p | J. Phys. Chem. Lett. 2014, 5, 2469−2473

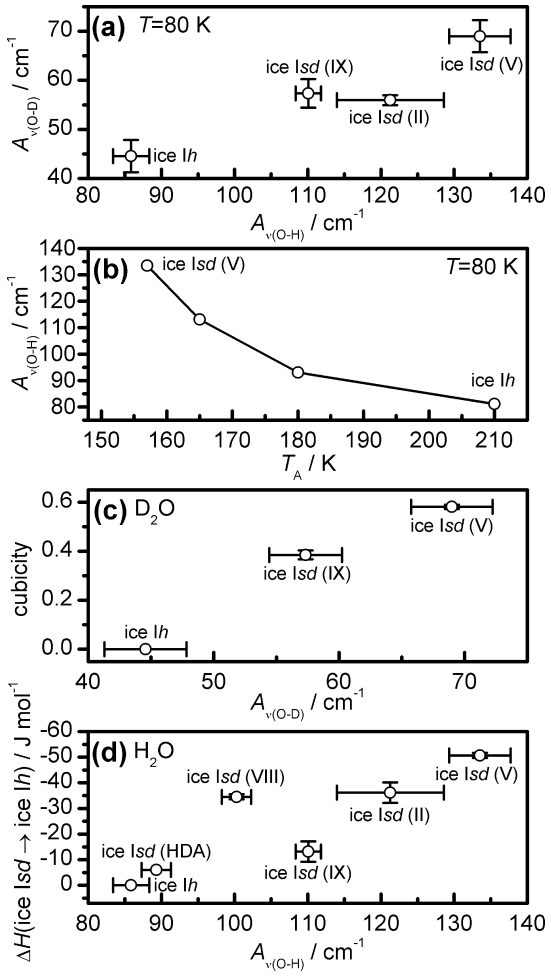

Figure 3. (a) Relationship between the integrated peak areas of the coupled ν(O−H) and ν(O−D) modes. (b) Changes in $A_{\nu(O-H)}$ as a function of the annealing temperature for ice I*sd* from ice V. (c) Cubicity values (175 K) from refs 8, 9, and 14, plotted against $A_{\nu(O-D)}$. (d) Ice I*sd* → ice I*h* phase transition enthalpies from refs 17, 20, and 34, plotted against $A_{\nu(O-H)}$.

symmetric stretching of water molecules vibrating in phase.[36,37] Whalley noted that at least 25 water molecules take part in this vibration in ice I*h*.[36] Due to the structural similarities between ice I*h* and ice I*sd*, we assume this value to be valid for ice I*sd* as well. Judging from the running coordination number shown in Figure 1b, it is therefore perfectly reasonable that the coupled stretching transitions in ice are affected by the fractions of cubic and hexagonal stacking.

As mentioned earlier, the presence of stacking disorder leads to a broadening of the symmetric stretching feature (cf. Figure 2). We propose that this is due to the structurally more diverse environments in which the water molecules vibrate in ice I*sd*. Regarding the intensity increases at the shoulders of the main peak, we suggest that they are associated with vibrational modes that appear as a consequence of the lower-symmetry environments created by the stacking disorder.

At this point, it is important to consider the relationship between the cubicity of an ice I sample and the corresponding degree of stacking disorder. For pure ice I*h*, the cubicity is zero, and there is no stacking disorder present. Upon increasing the cubicity from zero, the stacking disorder increases at first as the number of possible stacking arrangements grows. The most stacking disordered state is reached at a cubicity of $^1/_2$ for perfectly random stacking. Upon increasing the cubicity further, the stacking disorder decreases as the perfect ice I*c* structure is approached, which is free of stacking disorder.

At present, ice I*sd* samples well beyond the $^1/_2$ cubicity mark are not available or have not been characterized sufficiently (cf. Figure 3c). We emphasize that the spectroscopic trends reported here are thought to be mainly associated with stacking disorder and may not necessarily scale with cubicity. On the basis of the currently available spectroscopic data, it is difficult to make predictions about spectroscopic trends in the $^1/_2$ to 1 cubicity range.

The coupling of stretching transitions in ice can be "switched off" by introducing a small amount of O−D oscillators into H_2O ice (e.g., 2.5 w% D_2O in H_2O).[38] Unlike the coupled stretching transitions, the decoupled stretching modes, μ(O−D), are only influenced by the structure of the very local environment in ice. In Figure 4, it can be seen that the μ(O−D) of ice I*sd* from ice V is centered at a higher wavenumber and is broader compared to the μ(O−D) feature of ice I*h*. The larger half-width of the feature can again be explained by the presence of more diverse local environments in ice I*sd*. The shift to high wavenumbers indicates that the covalent O−D bonds are slightly stronger in ice I*sd* than those in ice I*h*. We suggest that the weaker covalent bonds in ice I*h* are caused by stronger hydrogen bonding or dispersive interactions (e.g., in the rings with boat conformation). In line with the results shown in Figure 3b, the μ(O−D) of ice I*sd* from ice V is consistent with that of ice I*h* after thermal annealing at 210 K.

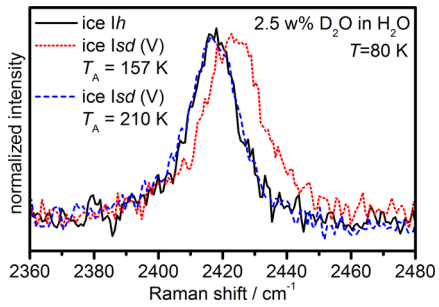

Figure 4. Normalized Raman spectra of the decoupled μ(O−D) region of H_2O ice I*sd* samples from ice V and ice I*h*, both containing 2.5 w% D_2O.

In summary, we have shown that Raman spectroscopy can be used for the detection of stacking disorder in ice I in a semiquantitative fashion. The results from our new method are in good agreement with data obtained from diffraction and calorimetric studies. Apart from gaining new fundamental insights into the spectroscopic properties of the ice I family, a new experimental method has now become available that may open up the door to identifying and characterizing ice I*sd* in nature. It has been shown that Raman spectroscopy can be adapted for remote and even telescopic applications in the 10−100 m range.[39,40] Furthermore, ground-based Raman LiDAR (light detection and ranging) instruments could potentially be used for detecting ice I*sd* in the Earth's atmosphere.[41] Such measurements would be very difficult to achieve with, for example, diffraction or calorimetry.

The advantage of studying ice I*sd* with diffraction is that absolute numbers for the cubicity of a sample can be obtained.[8−10,14] However, the presence of higher-order memory effects in the stacking sequence can make the analysis

dx.doi.org/10.1021/jz500996p | J. Phys. Chem. Lett. 2014, 5, 2469−2473

of diffraction patterns difficult. Furthermore, the various crystallographic parameters (stacking probabilities, lattice constants, peak profile parameters, etc.) are typically heavily correlated, which can result in large margins of error of the stacking probabilities. The potential of using calorimetry for characterizing ice I*sd* has not yet been fully explored. However, it has been noted that the heat released during the ice I*sd* to ice I*h* transition may be caused not only by changes from cubic to hexagonal stacking but also by sintering processes and increases in crystallite sizes.[20,42] Furthermore, due to the gradual nature of the ice I*sd* to ice I*h* transition, it is often difficult to choose the integration limits of the exothermic feature, and issues with contributions from the background signal can arise. To conclude, we believe that the combination of our new spectroscopic method with other techniques, such as diffraction and calorimetry, is now urgently needed to obtain a full understanding of the very complex nature of the metastable stacking disordered ice.

EXPERIMENTAL METHODS

The high-pressure phases of ice were prepared by compressing ice I*h* samples wrapped in indium foil to the required pressures at 77 K using a piston cylinder setup followed by isobaric heating. Once the target temperatures had been reached, the high-pressure phases were quenched using liquid nitrogen and recovered at ambient pressure. The target pressures and temperatures for the individual samples were: ice IX (0.3 GPa, 250 K), ice II (0.3 GPa, 235 K), ice V (0.6 GPa, 250 K), ice VIII (2.5 GPa, 270 K), and HDA (1.7 GPa, 77 K). The samples were then heated in an Oxford Microstat cryostat until complete conversion to ice I*sd* had taken place and immediately recooled to 80 K.

A Renishaw Ramascope spectrometer (632.8 nm) was used to record Raman spectra of the samples. The Raman shifts of all spectra were calibrated using the sharp emission lines of a neon discharge lamp.

AUTHOR INFORMATION

Corresponding Author

*E-mail: c.salzmann@ucl.ac.uk.

Notes

The authors declare no competing financial interest.

ACKNOWLEDGMENTS

We thank the Royal Society for a University Research Fellowship (C.G.S., UF100144), the EPSRC for a studentship (J.J.S.), and the Leverhulme Trust for a Research Grant (RPG-2014-04). We are also grateful to Benjamin J. Murray for discussions.

REFERENCES

(1) Mitra, S. *High-Pressure Geochemistry and Mineral Physics*; Elsevier: Amsterdam, The Netherlands, 2004.
(2) Yeh, Y.; Feeney, R. E. Antifreeze Proteins: Structures and Mechanisms of Function. *Chem. Rev.* **1996**, *96*, 601−618.
(3) Shamoto, T.; Tasaki, Y.; Okada, T. Chiral Ice Chromoatography. *J. Am. Chem. Soc.* **2010**, *132*, 13135−13137.
(4) Murray, B. J.; Knopf, D. A.; Bertram, A. K. The Formation of Cubic Ice under Conditions Relevant to Earth's Atmosphere. *Nature* **2005**, *434*, 202−205.
(5) Kwok, S. *Physics and Chemistry of the Interstellar Medium*; University Science Books: Sausalito, CA, 2007.
(6) König, H. Eine kubische Eismodifikation. *Z. Kristallogr.* **1943**, *105*, 279−286.
(7) Kuhs, W. F.; Bliss, D. V.; Finney, J. L. High-Resolution Neutron Powder Diffraction Study of Ice I_c. *J. Phys., Colloq.* **1987**, *48*, 631−636.
(8) Hansen, T. C.; Koza, M. M.; Kuhs, W. F. Formation and Annealing of Cubic Ice: I. Modelling of Stacking Faults. *J. Phys.: Condens. Matter* **2008**, *20*, 285104.
(9) Hansen, T. C.; Koza, M. M.; Lindner, P.; Kuhs, W. F. Formation and Annealing of Cubic Ice: II. Kinetic Study. *J. Phys.: Condens. Matter* **2008**, *20*, 285105.
(10) Malkin, T. L.; Murray, B. J.; Brukhno, A. V.; Anwar, J.; Salzmann, C. G. Structure of Ice Crystallized from Supercooled Water. *Proc. Natl. Acad. Sci. U.S.A.* **2012**, *109*, 1041−1045.
(11) Whalley, E. Cubic Ice in Nature. *J. Phys. Chem.* **1983**, *87*, 4174−4179.
(12) Shilling, J. E.; Tolbert, M. A.; Toon, O. B.; Jensen, E. J.; Murray, B. J. Measurements of the Vapor Pressure of Cubic Ice and Their Implications for Atmospheric Ice Clouds. *Geophys. Res. Lett.* **2006**, *33*, L17801.
(13) Moore, E. B.; Molinero, V. Is It Cubic? Ice Crystallization from Deeply Supercooled Water. *Phys. Chem. Chem. Phys.* **2011**, *13*, 20008−20016.
(14) Kuhs, W. F.; Sippel, C.; Falentya, A.; Hansen, T. C. Extent and Relevance of Stacking Disorder in "Ice Ic". *Proc. Natl. Acad. Sci. U.S.A.* **2012**, *109*, 21259−21264.
(15) Thürmer, K.; Nie, S. Formation of Hexagonal and Cubic Ice During Low-Temperature Growth. *Proc. Natl. Acad. Sci. U.S.A.* **2013**, *110*, 11757−11762.
(16) McMillan, J. A.; Los, S. C. Vitreous Ice: Irreversible Transformations During Warm-Up. *Nature* **1965**, *206*, 806−807.
(17) Handa, Y. P.; Klug, D. D.; Whalley, E. Difference in Energy Between Cubic and Hexagonal Ice. *J. Chem. Phys.* **1986**, *84*, 7009−7010.
(18) Yamamuro, O.; Oguni, M.; Matsuo, T.; Suga, H. Heat Capacity and Glass Transition of Pure and Doped Cubic Ices. *J. Phys. Chem. Solids* **1987**, *48*, 935−942.
(19) Mayer, E.; Hallbrucker, A. Cubic Ice from Liquid Water. *Nature* **1987**, *325*, 601−602.
(20) Handa, Y. P.; Klug, D. D.; Whalley, E. Energies of the Phases of Ice at Low Temperature and Pressure Relative to Ice I*h*. *Can. J. Chem.* **1988**, *66*, 919−924.
(21) Salzmann, C. G.; Mayer, E.; Hallbrucker, A. Thermal Properties of Metastable Ices IV and XII: Comparison, Isotope Effects and Relative Stabilities. *Phys. Chem. Chem. Phys.* **2004**, *6*, 1269−1276.
(22) Bertie, J. E.; Whalley, E. Infrared Spectra of Ices I*h* and I*c* in the Range 4000 to 350 cm^{-1}. *J. Chem. Phys.* **1964**, *40*, 1637−1645.
(23) Taylor, M. J.; Whalley, E. Raman Spectra of Ices I_h, I_c, II, III, and V. *J. Chem. Phys.* **1963**, *40*, 1660−1664.
(24) Bertie, J. E.; Calvert, L. D.; Whalley, E. Transformations of Ice II, Ice III, and Ice V at Atmospheric Pressure. *J. Chem. Phys.* **1963**, *38*, 840−846.
(25) Bertie, J. E.; Calvert, L. D.; Whalley, E. Transformations of ice VI and ice VII at Atmospheric Pressure. *Can. J. Chem.* **1964**, *42*, 1373−1378.
(26) Arnold, G. P.; Finch, E. D.; Rabideau, S. W.; Wenzel, R. G. Neutron-Diffraction Study of Ice Polymorphs. III. Ice Ic. *J. Chem. Phys.* **1968**, *49*, 4365−4369.
(27) Salzmann, C. G.; Radaelli, P. G.; Slater, B.; Finney, J. L. The Polymorphism of Ice: Five Unresolved Questions. *Phys. Chem. Chem. Phys.* **2011**, *13*, 18468−18480.
(28) Mishima, O.; Calvert, L. D.; Whalley, E. 'Melting Ice' I at 77 K and 10 kbar: A New Method of Making Amorphous Solids. *Nature* **1984**, *310*, 393−395.
(29) Minceva-Sukarova, B.; Sherman, W. F.; Wilkinson, G. R. The Raman Spectra of Ice (Ih, II, III, V, VI and IX) as Functions of Pressure and Temperature. *J. Phys. C* **1984**, *17*, 5833−5850.
(30) Wong, P. T. T.; Whalley, E. Raman Spectrum of Ice VIII. *J. Chem. Phys.* **1976**, *64*, 2359−2366.

(31) Klug, D. D.; Mishima, O.; Whalley, E. High-Density Amorphous Ice. IV. Raman Spectrum of the Uncoupled O−H and O−D Oscillators. *J. Chem. Phys.* **1987**, *86*, 5323−5328.
(32) Salzmann, C. G.; Loerting, T.; Klotz, S.; Mirwald, P. W.; Hallbrucker, A.; Mayer, E. Isobaric Annealing of High-Density Amorphous Ice between 0.3 and 1.9 GPa: In Situ Density Values and Structural Changes. *Phys. Chem. Chem. Phys.* **2006**, *8*, 386−397.
(33) Klug, D. D.; Handa, Y. P.; Tse, J. S.; Whalley, E. Transformation of ice VIII to Amorphous Ice by "Melting" at Low Temperature. *J. Chem. Phys.* **1989**, *90*, 2390−2392.
(34) Salzmann, C. G.; Kohl, I.; Loerting, T.; Mayer, E.; Hallbrucker, A. The Low-Temperature Dynamics of Recovered Ice XII as Studied by Differential Scanning Calorimetry: A Comparision with Ice V. *Phys. Chem. Chem. Phys.* **2003**, *5*, 3507−3517.
(35) Shephard, J. J.; Evans, J. S. O.; Salzmann, C. G. Structural Relaxation of Low-Density Amorphous Ice upon Thermal Annealing. *J. Phys. Chem. Lett.* **2013**, *4*, 3672−3676.
(36) Whalley, E. A Detailed Assignment of the O−H Stretching Bands of Ice I. *Can. J. Chem.* **1977**, *55*, 3429−3441.
(37) Whale, T. F.; Clark, S. J.; Finney, J. L.; Salzmann, C. G. DFT-Assisted Interpretation of the Raman Spectra of Hydrogen-Ordered Ice XV. *J. Raman Spectrosc.* **2013**, *44*, 290−298.
(38) Minceva-Sukarova, B.; Sherman, W. F.; Wilkinson, G. R. Isolated O−D Stretching Frequencies in Ice II. *Spectrochim. Acta, Part A* **1985**, *41*, 315−318.
(39) Klein, V.; Popp, J.; Tarcea, N.; Schmitt, M.; Kiefer, W.; Hofer, S.; Stuffler, T.; Hilchenbach, M.; Doyle, D.; Dieckmann, M. Remote Raman Spectroscopy as a Prospective Tool for Planetary Surfaces. *J. Raman Spectrosc.* **2004**, *35*, 433−440.
(40) Sharma, S. K. New Trends in Telescopic Remote Raman Spectroscopic Instrumentation. *Spectrochim. Acta, Part A* **2007**, *68*, 1008−1022.
(41) Neely, R. R.; Thayer, J. P. Raman Lidar Profiling of Tropospheric Water Vapor over Kangerlussuaq, Greenland. *J. Atmos. Oceanic Technol.* **2011**, *28*, 1141−1148.
(42) Johari, G. P. On the Coexistence of Cubic and Hexagonal Ice Between 160 and 240 K. *Philos. Mag. B* **1998**, *78*, 375−383.